From Quantum Fluctuations to Cosmological Structures
ASP Conference Series, Vol. 126, 1997
D. Valls-Gabaud, M. Hendry, P. Molaro and K. Chamcham (eds.)

7 : Gold in the Doppler Hills : Cosmological Parameters in the Microwave Background

C. H. Lineweaver
Observatoire Astronomique de Strasbourg,
11 Rue de l'Université, 67000 Strasbourg, France
charley@astro.u-strasbg.fr

Abstract. Research on the cosmic microwave background (CMB) is progressing rapidly. New experimental groups are popping up and two new satellites will be launched. The current enthusiasm to measure fluctuations in the CMB power spectrum at angular scales between 0.°1 and 1° is largely motivated by the expectation that CMB determinations of cosmological parameters will be of unprecedented precision: cosmological gold. In this Chapter I will try to answer the following questions:

- What is the CMB?
- What are cosmological parameters?
- What is the CMB power spectrum?
- What are all those bumps in the power spectrum?
- What are the current CMB constraints on cosmological parameters?

1. What is the cosmic microwave background ?

Thirty years ago Penzias and Wilson (1965) discovered excess noise in their horn antenna in Holmdel, New Jersey. The measured temperature of this noise was ~ 3 K and it did not vary in intensity over the sky; it was isotropic. They received the Nobel Prize for this serendipitous discovery of the cosmic microwave background (CMB) radiation. The prediction of the existence of a CMB and of its temperature (Alpher & Herman 1948) followed by its detection, provides possibly the strongest evidence for the Big Bang.

The observable Universe is expanding and cooling. Therefore in the past it was hotter and smaller. The CMB is the after-glow of thermal radiation left over from this hot early epoch. It is the redshifted relic of the Big Bang. The CMB is a bath of photons coming from every direction with wavelengths about as big as these letters. There are about 415 of them in every cubic centimeter of the Universe. These are the oldest photons one can observe (see Figure 1). Their long journey towards us has lasted 99.997% of the age of the Universe; a journey which began when the photons were last scattered by free electrons of the ubiquitous cosmic plasma, when the Universe was 1000 times smaller and the temperature 1000 times higher than the CMB is today. The CMB contains information about the Universe at redshifts much larger than the redshifts of galaxies or quasars. It is a unique tool for probing the early Universe.

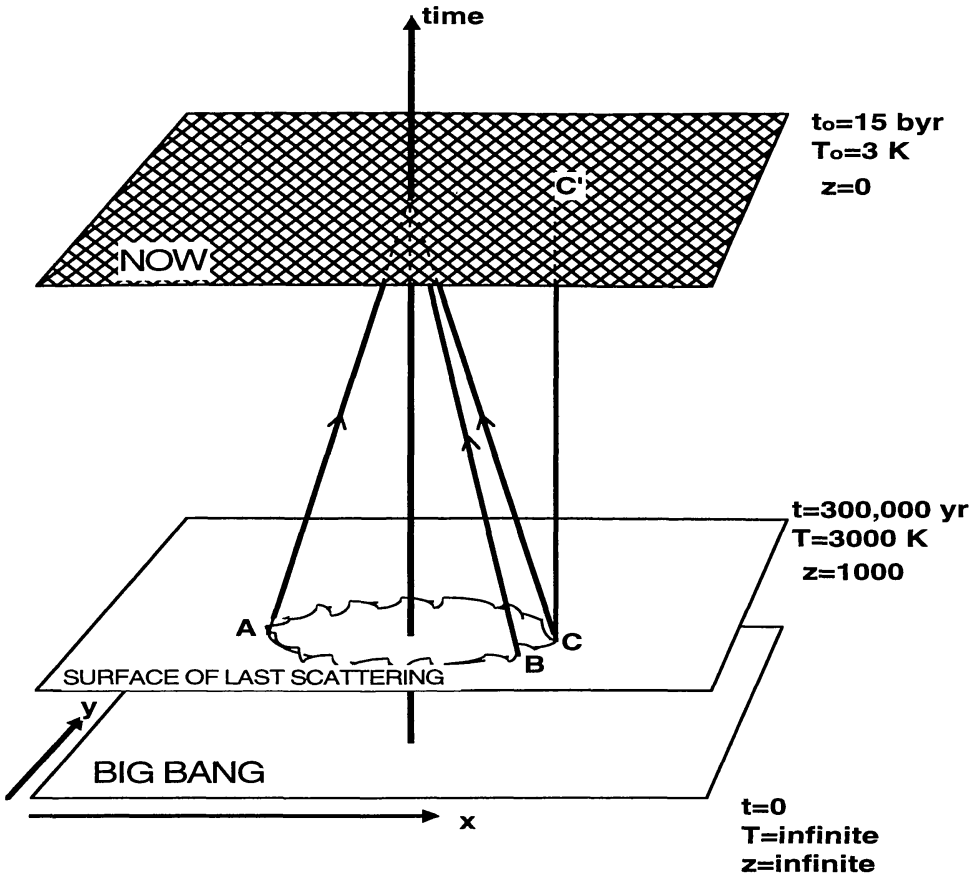

Figure 1. Comoving Space-Time and the Surface of Last Scattering. The time axis is the world line of the stationary observer who is currently located at the apex of the light cone. CMB photons travel from the wavy circle in the surface of last scattering along the surface of the light cone to the observer. Points A and C are on opposite sides of the sky. If the angle between B and C is greater than a few degrees then B and C have not been in (post-inflationary) causal contact. The unevenness of the circle represents potential fluctuations at the surface of last scattering. The bottom two planes are at fixed times while the "NOW" plane moves upward. As it does, the size of the visible Universe (diameter of the wavy circle) increases. The object seen at C is currently at C'. We are beginning to determine cosmological parameters by measuring the angular fluctuations in the temperature of the photons from the circle on the surface of last scattering. The surface of last scattering, or cosmic photosphere, is at a redshift of $z \approx 1000$ and is the boundary between the present cool transparent universe and the hot opaque Universe of the past. CMB photons are valuable fossils which have been studied by dozens of groups in efforts to more precisely determine their spectrum and spatial fluctuations. Since the most remote quasars are at $z \approx 5$, CMB structures at a redshift $z \approx 1000$ are also the most distant objects ever observed. Although very distant today, at the time they emitted the light, they were only $\sim 6\, h^{-1}$ Mpc away from us, closer than the Virgo cluster today. Figure from Lineweaver 1994.

To a very good approximation the CMB is a flat featureless blackbody; there are no anisotropies; the temperature is a constant in every direction ($T_o = 2.728 \pm 0.004\,\mathrm{K}$ (95% c.l.) Fixsen *et al.* 1996). This near isotropy was the reason it took more than 25 years to detect anisotropies in the CMB. However the galaxies around us are clustered on scales from 1 Mpc (our Local Group) up to $\sim$ 100 Mpc (great walls, sheets and voids). If these structures formed from overdensities which gravitationally collapsed, the overdensities must have been present in the early universe and must have produced temperature anisotropies in the CMB. In the Spring of 1992, the COBE DMR team announced the discovery of anisotropies in the CMB (Smoot *et al.* 1992). Since then the field of CMB-cosmology has blossomed.

2. What are cosmological parameters ?

2.1. Friedman Robertson Walker (FRW) universe

Cosmological parameters are the important ingredients of any cosmological model. If we work within General Relativity and add the hypothesis that the Universe is homogeneous and isotropic then the Einstein equations reduce to the Friedmann equation with its relatively few parameters:

$$\left(\frac{\dot{a}}{a}\right)^2 = H_0^2 \left[\frac{\Omega_{0,rel}}{a^4} + \frac{\Omega_{0,non-rel}}{a^3} + \frac{\Omega_{0,curv}}{a^2} + \frac{\Omega_\Lambda}{a^0}\right] \quad . \tag{7.1}$$

- **a**: the scale factor used to parametrize the global expansion (or shrinking) of the Universe. In the Big Crunch (or looking backwards towards the Big Bang) $a \to 0$.

- $\mathbf{H_0}$: the present value of Hubble's parameter. In terms of the scale factor $H_0 = (\dot{a}/a)_0$. The units are km s^{-1} Mpc^{-1} and it is sometimes written dimensionlessly as $h = H_0/(100\,\mathrm{km\ s^{-1}\ Mpc^{-1}})$. The subscript "0" refers to the present time.

- $\mathbf{\Omega_{0,i}}$: the current dimensionless density of component i of the Universe expressed in units of the critical density ($\rho_{crit} = 3H_0^2/8\pi G$). Thus for example the physical density of baryons is $\rho_b = \Omega_b\, \rho_{crit}$ and the measurement of ρ_b gives limits on $\Omega_b h^2$. The critical density marks the boundary between eternally expanding universes and recollapsing universes.

- $\mathbf{\Omega_{rel}}$: the density of relativistic matter, e.g., hot dark matter (HDM), neutrinos and radiation for which $pc > m_0c^2$. $\Omega_{rel} = \Omega_{HDM} + \Omega_\nu + \Omega_\gamma$.

- $\mathbf{\Omega_{non-rel}}$: the density of non-relativistic matter, e.g., cold dark matter (CDM) or baryons, $\Omega_{non-rel} = \Omega_{CDM} + \Omega_b$.

- $\mathbf{\Omega_0}$: the total matter density of the Universe, $\Omega_0 = \Omega_{0,rel} + \Omega_{0,non-rel}$.

- $\mathbf{\Omega_{curve}}$: the curvature density of the Universe. $\Omega_{0,curve} = -kc^2/H_0^2$. The factor $k \in [+1, 0, -1]$ for the cases of closed, flat or open geometries respectively, corresponding to $\Omega_0 + \Omega_\Lambda = [<1,\ 1,\ >1]$ respectively.

- $\mathbf{\Omega_\Lambda}$: vacuum density of the Universe. $\Omega_\Lambda = \rho_\Lambda/\rho_{crit} = \Lambda c^2/3H_0^2 = \Lambda c^2/3H_0^2$. The cosmological constant $\Lambda = 8\pi G\rho_\Lambda/c^2$.

Evaluating the Friedmann equation at the present ($a = a_0 = 1$) provides the constraint $\Omega_0 + \Omega_{0,curve} + \Omega_\Lambda = 1$. Inflation implies that the Universe is flat which means $\Omega_{curve} = 0$ and $\Omega_0 + \Omega_\Lambda = 1$. In the standard CDM model (flat universe, no cosmological constant, $\Omega_0 = 1 \approx \Omega_{0,non-rel} >> \Omega_{0,rel}$), Eq. (7.1) can be integrated to yield the age of the Universe $t_0 = 6.52\ h^{-1}$ Gyr. For more generic cases, $t_0 = f(h, \Omega_0, \Omega_\Lambda)$ (see e.g., Kolb & Turner 1990).

2.2. Perturbed FRW

An FRW universe is perfectly isotropic and homogeneous; a boring universe without galaxies, stars or dense perturbations like ourselves. So we need to add perturbations to the model. We parametrize these perturbations in terms of the normalization and slope of the CMB power spectrum. There are two families of perturbations which influence the CMB power spectrum: scalar (= density) perturbations and tensor (= gravitational wave) perturbations, and correspondingly there are 2 normalizations and slopes.

- $\mathbf{Q}$: the quadrupole normalization of the power spectrum, usually expressed in μK. Q was determined accurately by the COBE satellite. If $Q = 0$ there are no perturbations. Inflation does not predict this normalization. The tensor analog is $\mathbf{T}$.

- $\mathbf{n}$: the slope of the primordial power spectrum, observable today at the largest angles. The tensor analog is $\mathbf{n_T}$.

2.3. Summary

The perfectly homogeneous and isotropic FRW model is parametrized by

$$\mathbf{h,\ \Omega_0,\ \Omega_\Lambda,\ \Omega_{curve}} \quad . \tag{7.2}$$

The total mass density Ω_0 has several components which are also parameters:

$$\mathbf{\Omega_0} = [\mathbf{\Omega_{0,non-rel}}] + [\mathbf{\Omega_{0,rel}}] \tag{7.3}$$

$$= [\mathbf{\Omega_b + \Omega_{CDM}}] + [\mathbf{\Omega_{HDM} + \Omega_\nu + \Omega_\gamma}] \quad . \tag{7.4}$$

Perturbations to the FRW universe are parametrized by

$$\mathbf{n, n_T, Q, T} \quad . \tag{7.5}$$

Cosmological parameters are important because they tell us

- the ultimate destiny of the Universe: $f(\Omega_0, \Omega_\Lambda)$
- the age and size of the Universe: $f(h, \Omega_0, \Omega_\Lambda)$
- the composition of the Universe: $f(\Omega_b, \Omega_{CDM}, \Omega_{HDM}, \Omega_\nu, \Omega_\gamma)$
- the origin of structure

What makes these parameters even more important and what makes CMB-cosmology such a hot subject is that in the near future measurements of the CMB angular power spectrum will determine these parameters with the unprecedented precision of a few % (Jungman *et al.* 1996).

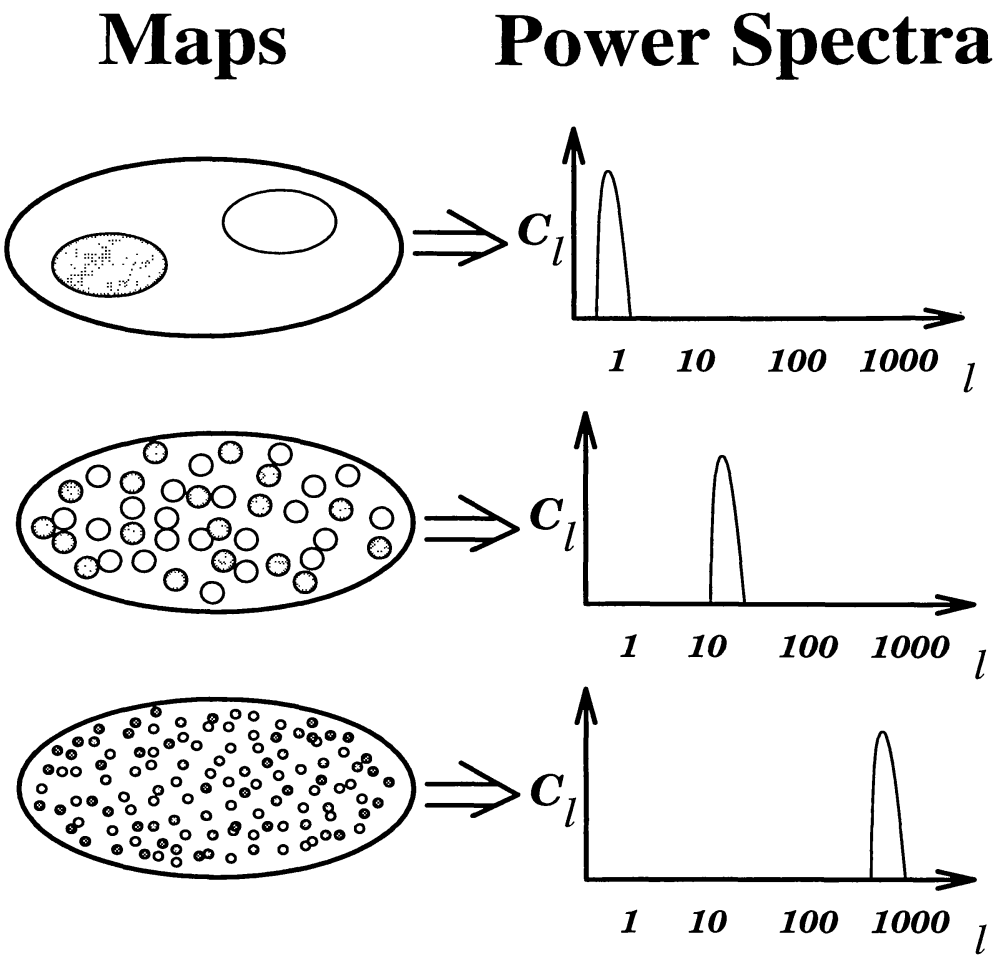

Figure 2. Simple maps and their power spectra. If a full-sky CMB map has only a dipole (top), its power spectrum is a delta function at $\ell = 1$. If a map has only temperature fluctuations on an angular scale of $\sim 7°$ (middle) then all of the power is at $\ell \sim 10$. If all the hot and cold spots are even smaller (bottom) then the power is at high ℓ.

3. What is the CMB power spectrum ?

Similar to the way sines and cosines are used in Fourier decompositions of arbitrary functions on flat space, spherical harmonics can be used to make decompositions of arbitrary functions on the sphere. Thus the CMB temperature maps are conveniently written as:

$$\Delta T(\theta, \phi) = \sum_{\ell,m} a_{\ell m} Y_{\ell m}(\theta, \phi) \quad . \tag{7.6}$$

The power spectrum is the sum of the squares of the coefficients

$$C_\ell = \frac{1}{2\ell + 1} \sum_m a_{\ell m}^2 \quad . \tag{7.7}$$

See Figure (2) for a brief C_ℓ initiation. If the matter power spectrum is written in scaleless form as $P(k) = A\,k^n$, then the radiation power spectrum at scales larger than a few degrees ($\ell \lesssim 20$) becomes (Bond & Efstathiou 1987)

$$C_\ell = Q^2 \frac{4\pi}{5} \frac{\Gamma(\ell + \frac{n-1}{2})}{\Gamma(\ell + \frac{5-n}{2})} \frac{\Gamma(\frac{9-n}{2})}{\Gamma(\frac{3+n}{2})} \quad , \tag{7.8}$$

where n is the slope of the power spectrum, Q^2 is the normalizing quadrupole amplitude (analogous to A and is just another way of writing C_2) and ℓ sets the angular scale (analogous to the linear scale k). If $n = 1$ (as implied by inflation, consistent with the COBE measurements and first proposed by Harrison (1970) and Zel'dovich (1972)), then

$$C_\ell = \frac{24\pi}{5} \frac{Q^2}{\ell(\ell+1)} \tag{7.9}$$

thus

$$\ell(\ell+1)C_\ell = \text{constant} \quad . \tag{7.10}$$

This is why the y-axis of CMB angular power spectra are labelled with some function of $\ell(\ell+1)C_\ell$ and why the plotted spectra are flat for $\ell \lesssim 20$ (see Figure 3).

3.1. Horizons and angular scales

To get a rough understanding of the power spectra in Fig. (3), we can divide up the plot into super-horizon and sub-horizon regions as is done in Figure (4). The angular scale corresponding to the particle horizon size is the boundary between super- and sub-horizon scales. The size of a causally connected region on the surface of last scattering is important because it determines the size over which astrophysical processes can occur. Normal physical processes can act coherently only over sizes smaller than the particle horizon and could not have produced the structure in the COBE maps and *a fortiori* could not have produced the better than one part in 10^4 homogeneity of the entire CMB sky.

A causally connected Hubble patch at last scattering subtends an angular size (for an observer today) of

$$\theta_H \approx 1^\circ\, \Omega_0^{1/2} \left(\frac{z_{dec}}{1000}\right)^{-1/2} \quad . \tag{7.11}$$

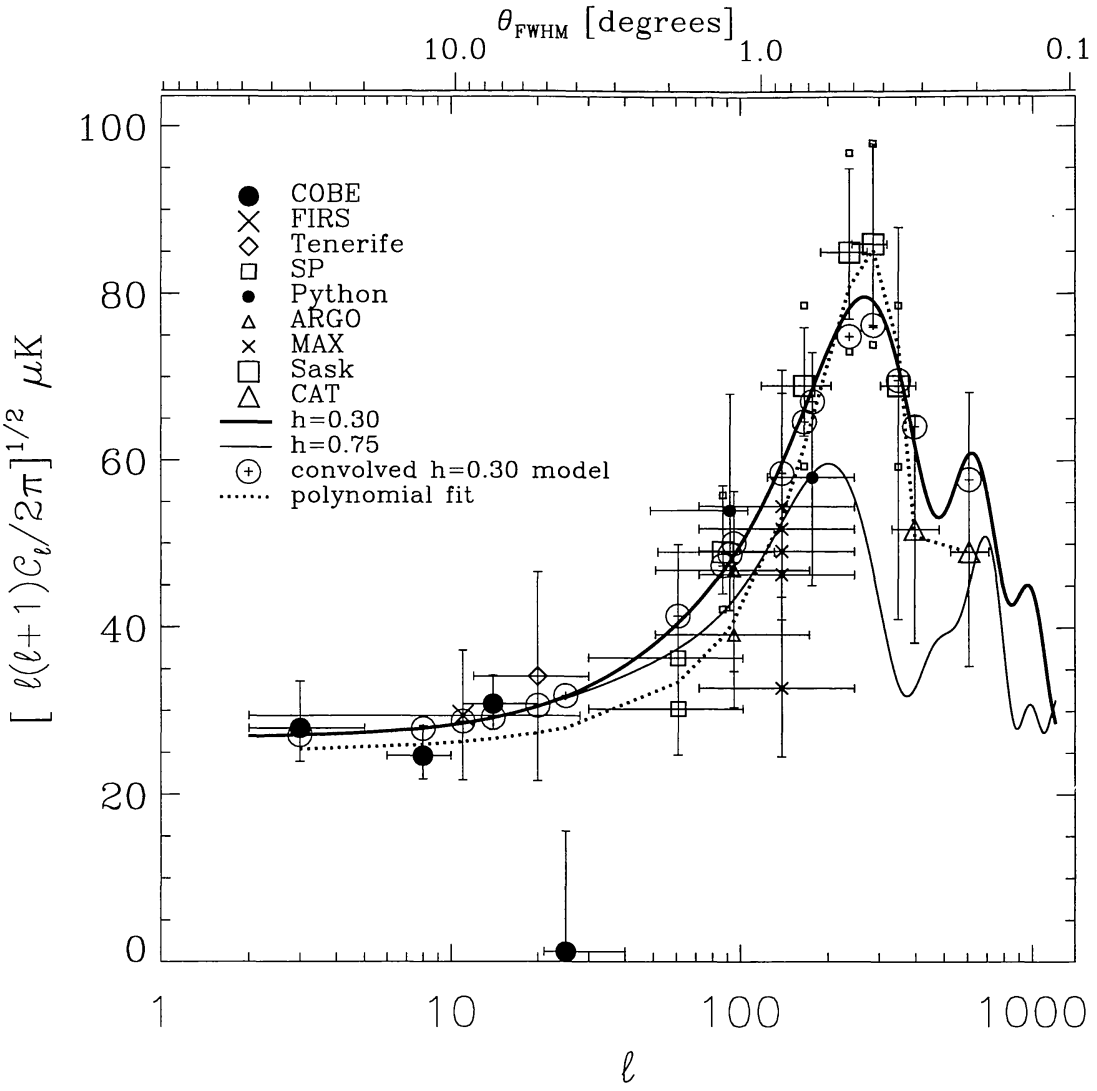

Figure 3. CMB Data. A compilation of 24 of the most recent measurements of the CMB angular power spectrum spanning the region $2 \lesssim \ell \lesssim 600$. COBE measurements are at the largest scales while the CAT interferometer measurements are at the smallest. Models with $h = 0.30$ and $h = 0.75$ are superimposed (both are $\Omega_0 = 1$, $\Omega_b = 0.05$, $n = 1$, $Q = 18$ μK). The low-h value is preferred by the data (see Figure 9). The dotted line is a 5th order polynomial fit to the data. Two satellites, MAP and Planck Surveyor, are expected to yield precise spectra for $\theta_{FWHM} \gtrsim 0°.3$ ($\ell \lesssim 400$) and $\theta_{FWHM} \gtrsim 0°.2$ ($\ell \lesssim 700$) respectively. The angular scale is marked at the top. Figure from Lineweaver *et al.* (1997a).

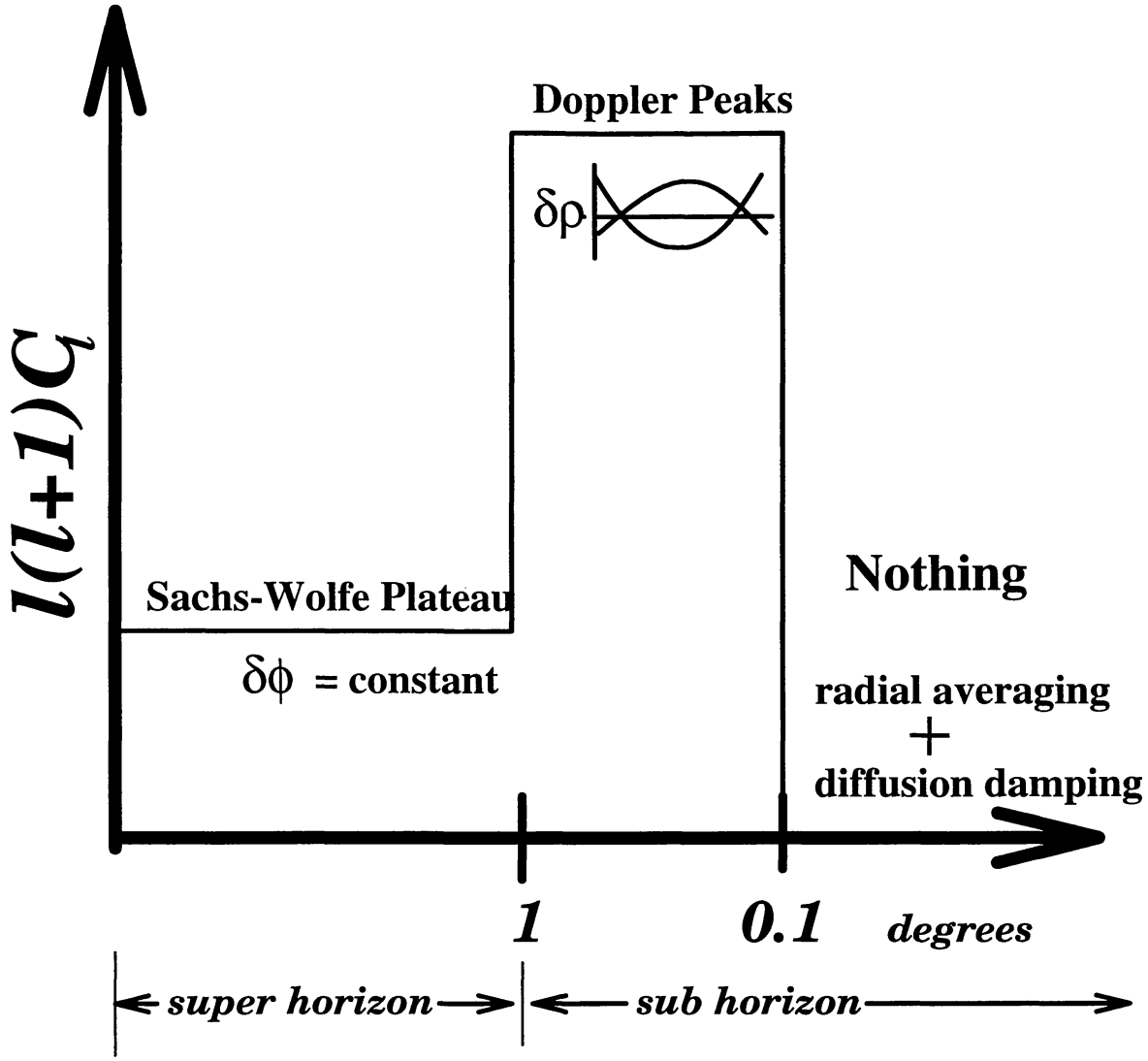

Figure 4. Simplified CMB power spectrum. The CMB power spectrum can be crudely divided into three regions. The Sachs-Wolfe plateau caused by the scale independence of gravitational potential fluctuations which dominate the spectrum at large super-horizon scales. The horizon is the angular scale corresponding to ct_{dec} where c is the speed of light and t_{dec} is the age of the Universe at decoupling. The Doppler peaks on scales slightly smaller than the horizon are due to resonant acoustic oscillations analogous to mellifluous bathroom singing (see Figure 8). At smaller scales there is nothing because the finite thickness of the surface of last scattering averages small scale fluctuations along the line of sight. Diffusion damping (photons diffusing out of small scale fluctuations) also suppresses power on these scales.

Thus as $\Omega_0 \uparrow$, $\theta_H \uparrow$ and as $z_{dec} \uparrow$, $\theta_H \downarrow$ (see Figure 5). The angle θ subtended by an object of size ct at an angular distance d_{ang} is $\theta \sim ct/d_{ang}$. Thus the angular scale associated with the peak of the power spectrum is

$$\ell_{peak} \sim \frac{1}{\theta_{peak}} \sim \frac{d_{ang}(h, \Omega_0, \Omega_\Lambda)}{c\, t_{dec}} \sim \frac{h^{-1} f(\Omega_0, \Omega_\Lambda)}{(\Omega_0 h^2)^{-1/2}} \sim \frac{f(\Omega_\Lambda)}{h} \quad , \tag{7.12}$$

where θ_{peak} is the angular scale of the Doppler peak. The physical scale of the peak oscillations is some fixed fraction of the horizon $\propto c\ t_{dec}$. The time of decoupling scales as $(\Omega_0 h^2)^{-1/2}$ and the angular distance $d_{ang} = h^{-1} f(\Omega_0, \Omega_\Lambda)$. In flat models $\Omega_0 = 1 - \Omega_\Lambda$ and $f(\Omega_0, \Omega_\Lambda) \rightarrow f(\Omega_\Lambda)$ where

$$f(\Omega_\Lambda) = \int_0^{z_{dec}} \frac{dz}{[(1+z)^3 - \Omega_\Lambda (1+z)^3]^{1/2}} \quad . \tag{7.13}$$

Inserting this into Eq. (7.12) yields the monotonic relation: when $\Omega_\Lambda \uparrow$, $\ell_{peak} \uparrow$ (see Figure 5b). Equation (7.12) says that when $\frac{f(\Omega_\Lambda)}{h} \uparrow \ell_{peak} \uparrow$. The h scaling can be understood as the effect of larger universes: a given physical size at a larger distance subtends a smaller angle (see Figures 5 and 5b).

There is structure in the DMR maps on super-horizon scales. How did it get there? Inflation is invoked to explain this apparently acausal structure (see the contribution by Liddle in Chapter 2.). If defect models of structure formation are correct then this acausality is only apparent; low z defects produced the large scale anisotropies. If inflation is correct, the apparent causal disconnection of the spots in the DMR maps means we are looking much further back than the epoch of last scattering. The structure that one sees in the DMR maps may represent a glimpse of quantum fluctuations at the inflationary epoch $\sim 10^{-32}$ seconds after the Big Bang, showing us scales $\sim 10^{16}$ times smaller than the atomic structure seen with the best ground-based microscopes. For more on the DMR instrument as a microscope see Lineweaver (1995).

4. What are all those bumps in the power spectrum ?

4.1. Decoupling and the surface of last scattering

At about 300,000 years after the bang, the Universe had cooled down enough to allow the free electrons and protons to combine to form neutral hydrogen. This period is known as decoupling. This neutralization of the plasma allowed photons to free stream in all directions. Before decoupling the Universe was an opaque fog of free electrons, afterwards it was transparent. The boundary is called decoupling, recombination, the cosmic photosphere or the surface of last scattering; the surface where the CMB photons were Thomson scattered for the last time before arriving in our detectors.

Decoupling occurs when the CMB temperature has dropped to the point when there are no longer enough high energy photons in the CMB to keep hydrogen ionized; $\gamma + H \leftrightarrow e^- + p$. Although the ionization potential of hydrogen is 13.6 eV ($T \sim 10^5$ K) decoupling occurs at $T \approx 3000$ K. The high photon to proton ratio ($\eta \approx 10^9$) allows the high energy tail of the Planck distribution to

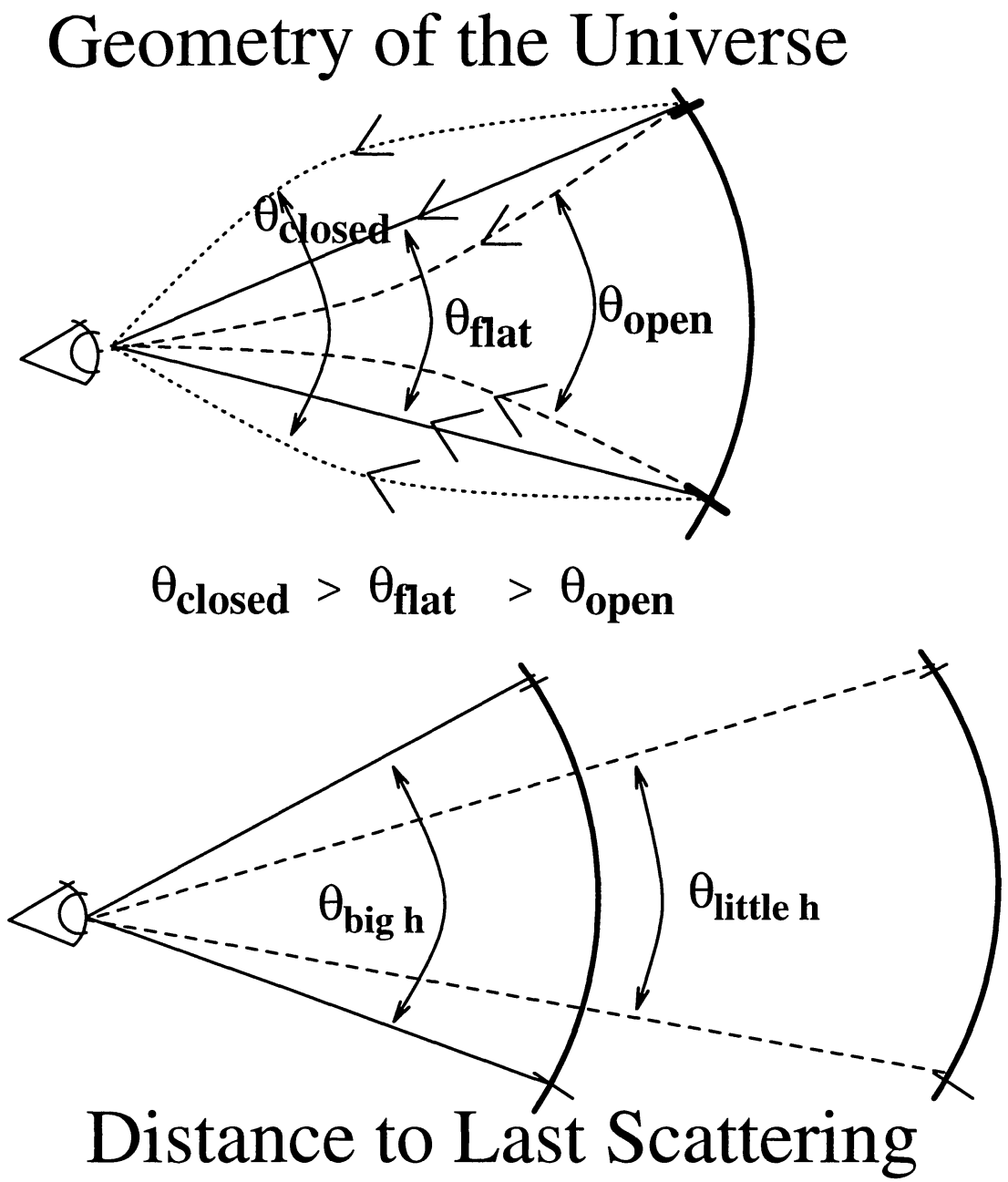

Figure 5. Effects of geometry and distance. Observers are on the left. The surface of last scattering is the thick curved line on the right. In the top panel, the same physical scale (on the right) subtends different angular scales depending on the geometry. In closed universes (geometry of the surface of a sphere, $\Omega_0 + \Omega_\Lambda > 1$, $k = +1$), the angle is largest. In open universes (geometry of the surface of a saddle, $\Omega_0 + \Omega_\Lambda < 1$, $k = -1$), the angle is smallest. In flat universes (Euclidean geometry of a plane, $\Omega_0 + \Omega_\Lambda = 1$, $k = 0$), the angle is between the other two. In the flat universe of the bottom figure, the angle subtended by a given physical scale depends on the distance to the surface of last scattering (see Section 3.1.). Summary: all the features of the power spectrum are shifted to smaller scales in open universes and for small h.

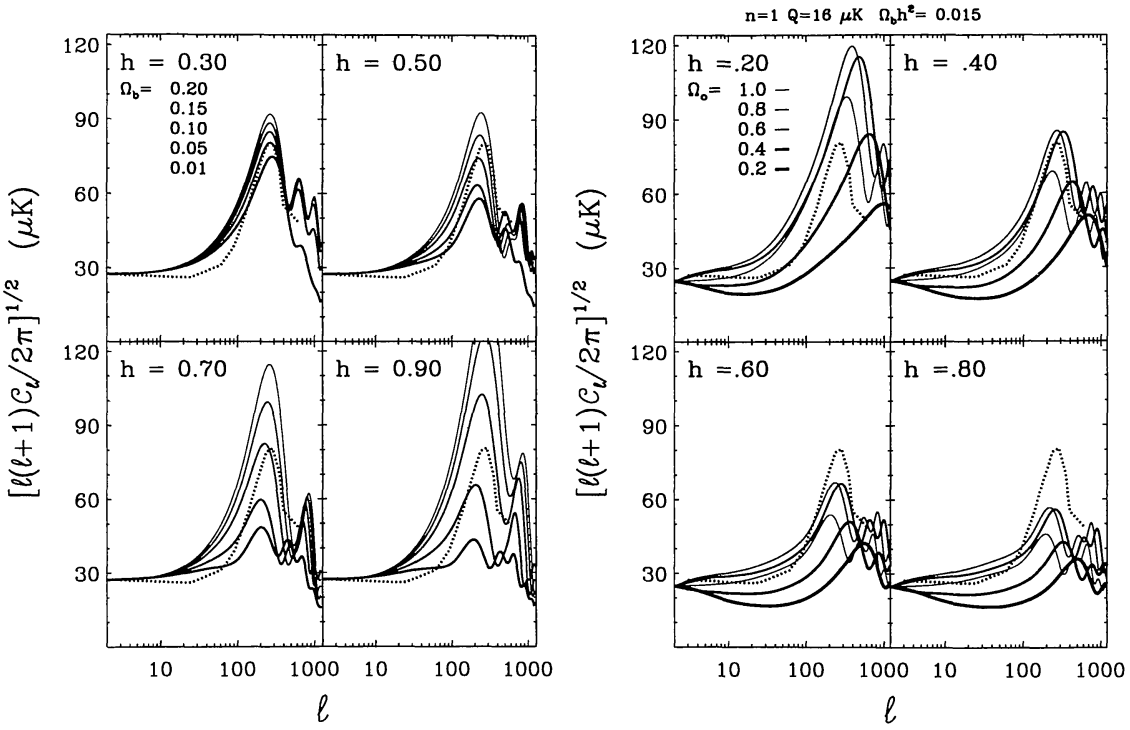

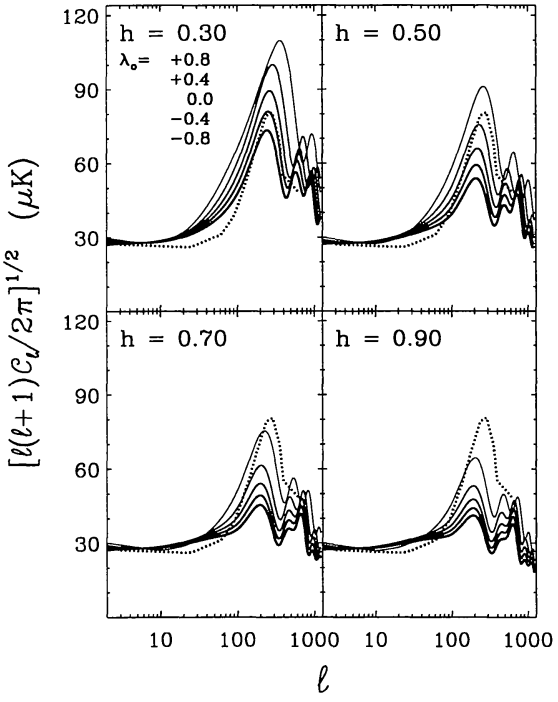

Figure 5b. Power spectra parameter dependence. The dotted line is the polynomial fit to the data in Figure 3 and is the same in all panels as a reference. Top left: in each panel h is fixed while Ω_b takes on the values indicated. The largest values of Ω_b have the largest Doppler peaks. Notice that as h increases, the peak amplitude increases for large Ω_b but decreases for small Ω_b; thus at high h the peak amplitude is an excellent baryometer. Upper right: in each panel Ω_0 takes on the values indicated. Notice that the slope at low ℓ and the peak amplitude do not have a simple monotonic dependence on Ω_0. Lower left: in each panel Ω_Λ takes on the values indicated. The largest values of Ω_Λ have the largest Doppler peaks. As h increases, the peak amplitude decreases and the peak position shifts to larger scales. All models are Harrison Zel'dovich ($n = 1$) normalized to the COBE 4-year results. Figures from Lineweaver *et al.* 1997a, Lineweaver & Barbosa 1997.

keep the comparatively small number of hydrogen atoms ionized until this much lower temperature (for details check out the Saha equation).

The temperature of the CMB as a function of redshift is $T(z) = T_0(1+z)$. Decoupling occurs at a fixed temperature $T(z_{dec}) =$ constant. As the universe cools down $T_0 \downarrow$, thus the surface of last scattering recedes from us with an ever-increasing redshift, $z_{dec} \propto 1/T_0(t)$.

4.2. Anisotropy mechanisms in a perturbed Robertson-Walker universe

The temperature of CMB photons can be influenced by any field which couples to photons. There are three:

- Gravity $\phi(\vec{r})$, by gravitational red and blue shifts
- Density $\rho(\vec{r})$, by compression heating and rarefaction cooling
- Velocity $v(\vec{r})$, by scattering from moving charged particles (Doppler effect).

The dominant effects on the CMB produced by these fields occur at the surface of last scattering, i.e., at a distance $|\vec{r}| \approx 6000\ h^{-1}$ Mpc from the observer in the direction of the line of sight (Figure 6). The differential temperature of the CMB in direction $\vec{r}$, $\delta T(\vec{r}) = T(\vec{r}) - T_0$, can be expressed as a function of the potential ϕ, the density fluctuations δ and the velocity $\vec{v}$.

$$\frac{\delta T(\vec{r})}{T_o} = \frac{\phi(\vec{r})}{c^2} + \frac{1}{3}\delta(\vec{r}) - \vec{r}\cdot\frac{\vec{v}(\vec{r})}{c} + \frac{2}{c^2}\int \dot{\phi}(\vec{r},t)\,dt \quad , \tag{7.14}$$

or in words,

$$Temperature = Gravity + Density + Velocity + Changing\ Gravity. \tag{7.15}$$

Notice that all four terms in Eq. (7.14) are independent of the frequency of the radiation. This spectral flatness is used by observers to distinguish CMB anisotropies from Galactic and extragalactic foregrounds. In the next two pages I will try to explain how these different terms influence the CMB on different scales.

4.3. Large super-horizon scales

• Gravity

On angular scales larger than a few degrees, the cold and hot spots in the CMB maps are caused by the red- and blue-shifting of photons leaving primordial gravitational potential fluctuations (Sachs & Wolfe 1967). That is, photons at the surface of last scattering lose energy climbing out of potential valleys and gain energy falling down potential hills; and these valleys and hills have different amplitudes as a function of position on the sky. Hills produce hot spots while valleys produce cold spots. The Pound-Rebka experiment used the Mossbauer effect and confirmed the existence of a gravitational redshift of magnitude ϕ/c^2, the first term of Eq. (7.14).

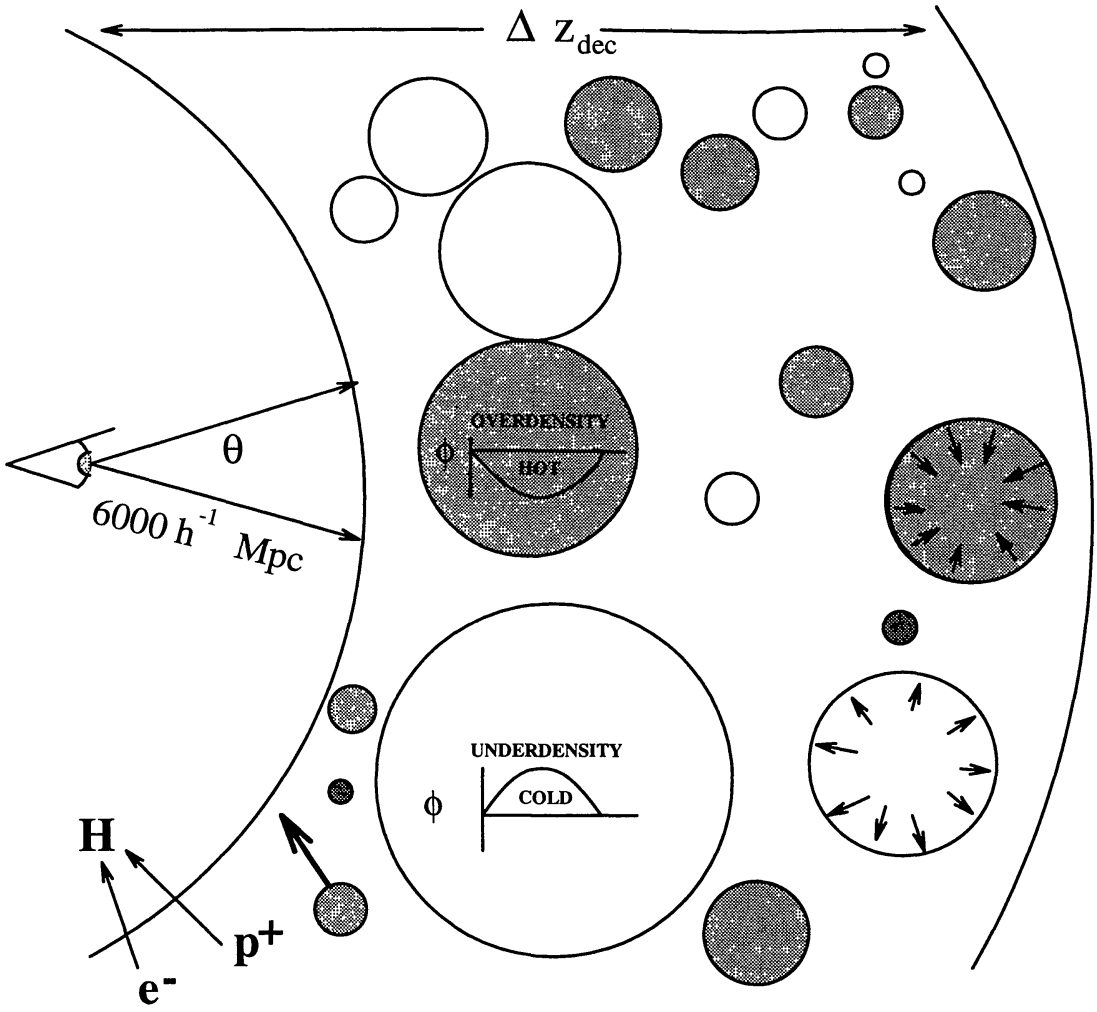

Figure 6. Fluctuation production at last scattering. Gravity (ϕ), density (ρ) and velocity (v) fields couple to the CMB photons and produce temperature anisotropies at the surface of last scattering. The grey circles are hot potential wells and the white circles are cool potential hills. Adiabatic conditions specify that the locations of the CDM potential wells coincide with the positions of the baryon-photon overdensities, and potential hills coincide with the baryon-photon underdensities. In climbing out of the potential wells, the initially hot photons become gravitationally redshifted and end up cooler than average. Similarly, in falling down the potential hills, the initially cooler photons become hotter than average. Thus on the largest scales (where these two effects dominate) the cool spots in the COBE maps are regions of overdensity. Bulk velocities of the plasma are indicated by the arrow on the grey spot in the lower left but are not expected on super horizon scales. On horizon scales, matter is falling into potential wells and falling down potential hills analogous to the bulk flow velocities measured in local pre-virialized objects. Acoustic velocities are indicated by the radial arrows in the well and hill on the right (see Fig. 8).

• Density

The initial conditions are usually selected to be adiabatic and less commonly isocurvature. With adiabatic initial conditions the locations of the overdensities in the baryon-photon fluid coincide with the locations of the potential wells. This leads to a partial cancelling of the gravity and density terms (see Fig. 6). On super-horizon scales $\delta \approx -2\phi/c^2$, thus the sum of the gravity and density terms is $\phi/3c^2$ (gravity wins).

With isocurvature initial conditions the curvature from CDM potential wells is compensated by coinciding underdensities of the baryon-photon fluid. No curvature (= "isocurvature") is the result. The gravity and density terms do not cancel, in fact they add coherently leading to relatively more power on super-horizon scales compared to the adiabatic case.

• Velocity

The $\vec{r}\cdot\vec{v}(\vec{r})/c$ term is the standard Doppler effect applied to radiation. The velocity can be conveniently decomposed

$$\vec{v}(\vec{r}) = \vec{v}_\odot + \vec{v}_{dec}(\vec{r}) \quad , \tag{7.16}$$

where $\vec{v}_\odot$ is the velocity of the observer, i.e., the velocity of the Sun with respect to the CMB and $\vec{v}_{dec}$ is the velocity of the last scattering plasma with respect to the CMB. The Doppler term from $\vec{v}_\odot$ produces the large observed dipole, known also as the "Great Cosine in the Sky". The measurement of this dipole tells us how fast we are moving with respect to the rest frame of the CMB (Lineweaver *et al.* 1995; Lineweaver *et al.* 1996). When we make a CMB map and remove the mean, the next largest feature visible at 1000 times smaller amplitude is the dipole. But the amplitude of this kinetic dipole is $\sim$ 100 **larger** than the anisotropies of the CMB power spectrum.

On large scales Eq. (7.14) becomes

$$\frac{\delta T(\vec{r})}{T_0} = \frac{\phi(\vec{r})}{3c^2} - \frac{\vec{r}\cdot\vec{v}_\odot}{c} \quad . \tag{7.17}$$

When we remove the dipole from the maps we are left with only the combined gravity/density term of the Sachs-Wolfe effect, $\phi/3c^2$.

On super-horizon scales, the physical decomposition we are making here is ambiguous, i.e., gauge dependent. One gauge's adiabatic compression is another gauge's gravitational redshift, but the observed $\delta T(\vec{r})/T_0$ is gauge independent (see e.g. Hu 1995).

4.4. Small sub-horizon scales

• Gravity

The integrated Sachs-Wolfe effect (ISW) is gravitational redshifting when the CMB photons fall into shallow potential valleys and climb out of deep valleys (Figure 7).

The early ISW effect is due to the self-gravity of the photons just after z_{dec}. Since photon potentials do not grow with the same scaling as the non-relativistic matter, $\dot{\phi} \neq 0$. Near decoupling, $\Omega_\gamma(z \sim z_{dec})$ is non-negligible and if we let $h \to 0.20$, $z_{eq} \to z_{dec}$, which means that Ω_γ is larger at decoupling and that the contribution from the early ISW effect increases.

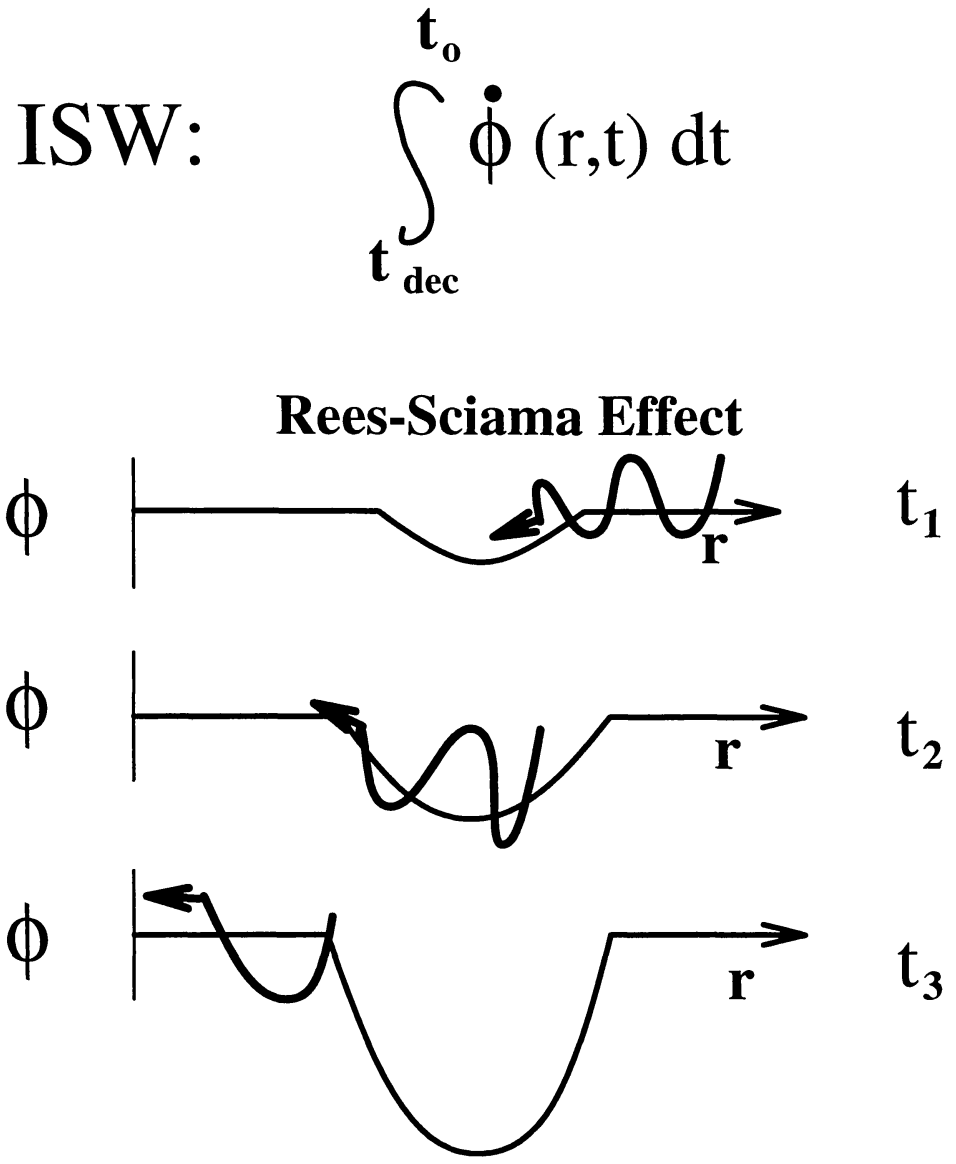

Figure 7. Integrated Sachs-Wolfe (ISW) effect. Consider an overdensity that is growing such as a collapsing proto-cluster of galaxies. CMB photons cross such structures on their way to us. Falling into a shallow potential well and then climbing out of it when it is deeper results in a net redshift of the photons. This is known as the Rees-Sciama effect and is a specific case of the more generic integrated Sachs-Wolfe (ISW) effect.

The late ISW effect is also from $\dot{\phi} \neq 0$ and is produced in non-flat universes ($k \neq 0$) or when $\Lambda \neq 0$. It is "late" in the sense that in the limit as $a \to \infty$ (late times) the last two terms in the Friedmann equation control the expansion (see Tegmark 1995, and Hu 1995 for more details).

After matter-radiation equality, the growth of CMB potential wells and hills drives acoustic oscillations (see Figure 8).

• Density

The correlated combination of density and velocity fluctuations are acoustic waves. Since we are dealing essentially with a single baryon-photon fluid, (the electrons couple the baryons tightly to the photons) adiabatic compression and rarefaction of this fluid creates hot and cold spots that can be seen (Fig. 8).

• Velocity

Plasma at the surface of last scattering can have a velocity due to bulk motions or to acoustic oscillations which are 90 degrees out of phase with density fluctuations. Fig. (8) displays these acoustic oscillations at different scales.

For simplicity, in Eq. (7.14), we have assumed a Robertson-Walker metric and therefore do not consider differential expansion as a source of anisotropy. Additionally, we do not include the Vishniac (1987) and Sunyaev-Zel'dovich (1969) effects. These post-decoupling effects contribute to small angular scale anisotropies. We also do not include the more speculative anisotropies due to topological defects (monopoles, strings, walls, textures) or any contribution from a possible rotation of the Universe (Barrow, Juszkiewicz & Sonoda 1985). We also do not include polarization anisotropies. For excellent reviews of this subject and more details see Tegmark (1995), Hu (1995), Bunn (1997) and Hu, Sugiyama & Silk (1997).

5. What are the current CMB constraints on cosmological parameters ?

The current enthusiam to measure fluctuations in the CMB power spectrum at angular scales between $0.^{\circ}1$ and 1° is largely motivated by the expectation that CMB determinations of cosmological parameters will be of unprecedented precision. In such circumstances it is important to estimate and keep track of what we can already say about the cosmological parameters. In two recent papers (Lineweaver *et al.* 1997a,b) we have compiled the most recent CMB measurements, used a fast Boltzmann code to calculate model power spectra (Seljak & Zaldarriaga 1996) and, with a χ^2 analysis, we have compared the data to the power spectra from several large regions of parameter space.

In Lineweaver *et al.* (1997a) we considered COBE-normalized flat universes with $n = 1$ power spectra. We used predominantly goodness-of-fit statistics to locate the regions of the $h - \Omega_b$ and $h - \Lambda$ planes preferred by the data. In Lineweaver & Barbosa (1997) we obtained χ^2 values over the 4-dimensional parameter space $\chi^2(h, \Omega_b, n, Q)$ for $\Omega = 1$, $\Lambda = 0$ models. Projecting and slicing this 4-D matrix gives us the error bars around the minimum χ^2 values. Here we summarize several of our most important results.

One of the difficulties in this analysis is the 14% absolute calibration uncertainty of the 5 important Saskatoon points which span the dominant adiabatic peak in the spectrum (Fig. 3). We treat this uncertainty by doing the analysis three times: all 5 points at their nominal values ('Sk0'), with a 14% increase ('Sk+14') and a 14% decrease ('Sk-14'). Sk+14 and Sk-14 are indicated by the small squares in Fig. (3) above and below the nominal Saskatoon points. Leitch *et al.* (1997) report a preliminary relative calibration of Jupiter and Cas A implying that the Saskatoon calibration should be $-1\% \pm 4\%$. Reasonable χ^2 fits are obtained for Sk0 and Sk-14.

In the context of the flat models tested, our χ^2 analysis yields: $H_0 = 30^{+13}_{-9}$ (Fig. 9), $n = 0.93^{+0.17}_{-0.16}$ and $Q = 17.5^{+3.5}_{-2.5}\,\mu$K (Fig. 10). The n and Q values are consistent with previous estimates while the H_0 result is surprisingly low.

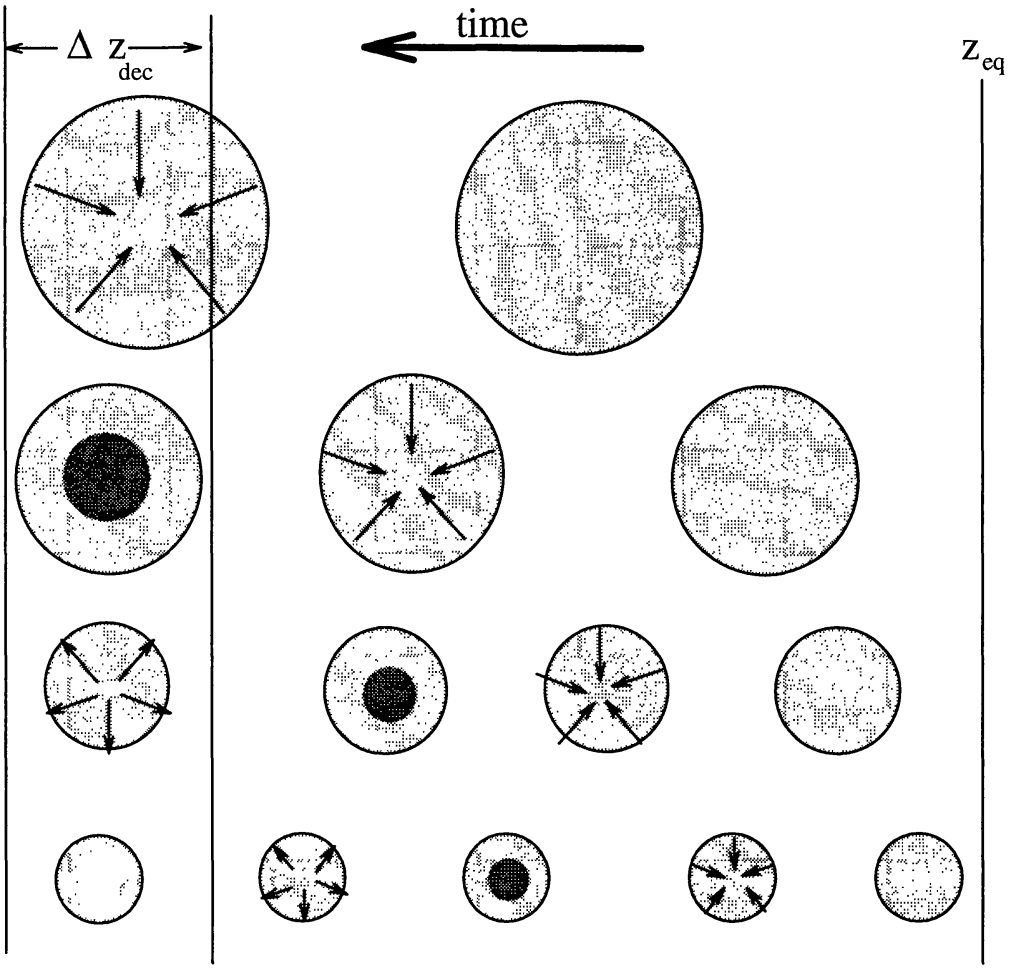

Figure 8. Seeing acoustic oscillations. The grey spots are CDM potential wells of four different sizes evolving in time. The arrows represent velocities of the baryon-photon fluid. After z_{eq}, in the matter dominated era, the baryon-photon fluid can begin to collapse into potential wells which enter the horizon. Acoustic oscillations on scales smaller than the sound horizon can begin to oscillate. The imprint of these acoustic oscillations is left in the CMB photons when the Universe becomes transparent during the period marked Δz_{dec}. Thus we see acoustic oscillations in the snap-shot of the Universe called the surface of last scattering. The top row corresponds to the largest scale Doppler contribution and contributes power at scales slightly larger than the main acoustic peak (few degrees). It is caught at decoupling with maximum velocity. The second row corresponds to the main acoustic peak in the power spectrum at an angular scale of $\sim 0.^{\circ}5$ (see Fig. 3). This is inappropriately called the "Doppler peak". It is caught at maximum compression (= hot) when the velocities are minimal. Potential hills of the same size (not shown here) produce a rarefaction peak (= cold). The third row is the second Doppler peak which fills in the first valley of the power spectrum ($\sim 0.^{\circ}3$). The last row is the second acoustic peak ($\sim 0.^{\circ}2$). It is a rarefaction peak (= white spot) for potential wells and a compression peak for potential hills (not shown here). The compression/rarefaction peaks are 90° out of phase with the velocity peaks.

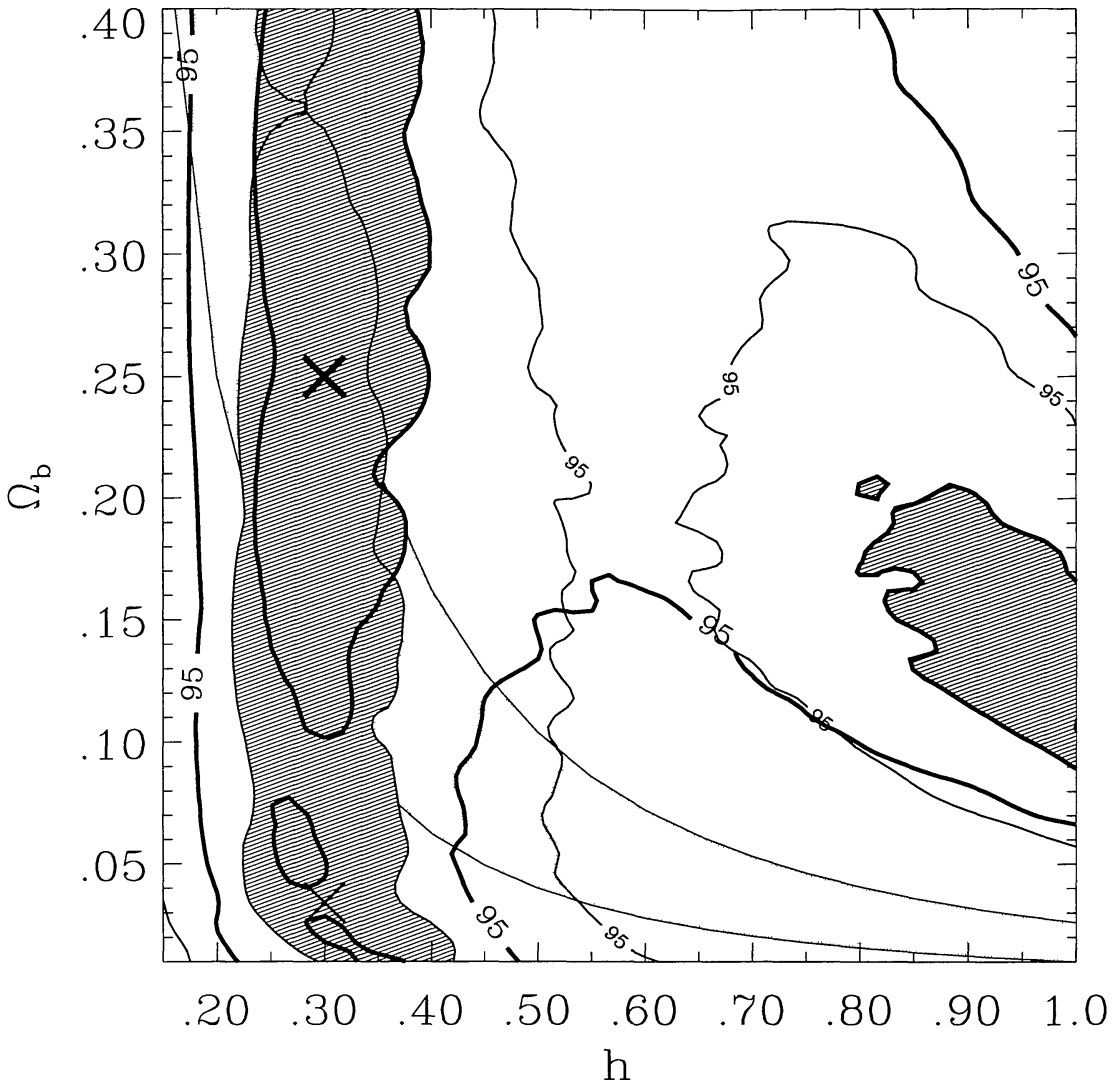

Figure 9. Constraints on Hubble's constant. The dark grey areas denote the regions of parameter space favored by the CMB data. They are defined by $\chi^2_{min} + 1$ for Sk0 and Sk-14 (minima marked with thick and thin 'X' respectively) (cf. Section 5.). '95' denotes the $\chi^2_{min} + 4$ contours for Sk0 (thick) and Sk-14 (thin). The light grey band is from Big Bang nucleosynthesis ($0.010 < \Omega b\, h^2 < 0.026$). The parameters n and Q have been marginalized. In the H_0 result quoted, we neglect the region at $H_0 \sim 100$ with $\Omega_b \sim 0.15$. This figure shows clearly that lowering the calibration by 14% **does not** favor higher values of H_0. Figure from Lineweaver & Barbosa 1997.

For each result, the other 3 parameters have been marginalized. This H_o result has a negligible dependence on the Saskatoon calibration, i.e., lowering the Saskatoon calibration from 0 to −14% does not raise the best-fitting H_0 in flat models. The inconsistency between this low H_0 result and $H_0 \sim 65$ results will not easily disappear with a lower Saskatoon calibration. Our results are valid for the specific models we considered: $\Omega = 1$, CDM dominated, $\Lambda = 0$, Gaussian adiabatic initial conditions, no tensor modes, no early reionization, $T_o = 2.73$ K, $Y_{He} = 0.24$, no defects, no HDM.

There are many other cosmological measurements which are consistent with such a low value for H_0 (Bartlett *et al.* 1995; Liddle *et al.* 1996). For example, we calculated a joint likelihood based on the observations of galaxy cluster baryonic fraction, Big Bang nucleosynthesis and the large scale density fluctuation shape parameter, Γ. We obtained $H_0 \approx 35^{+6}_{-5}$.

With two new CMB satellites to be launched in the near future (MAP $\sim$ 2001, Planck Surveyor $\sim$ 2005) and half a dozen new CMB experiments coming on-line (23 groups), the future looks bright for CMBers (see Page 1997).

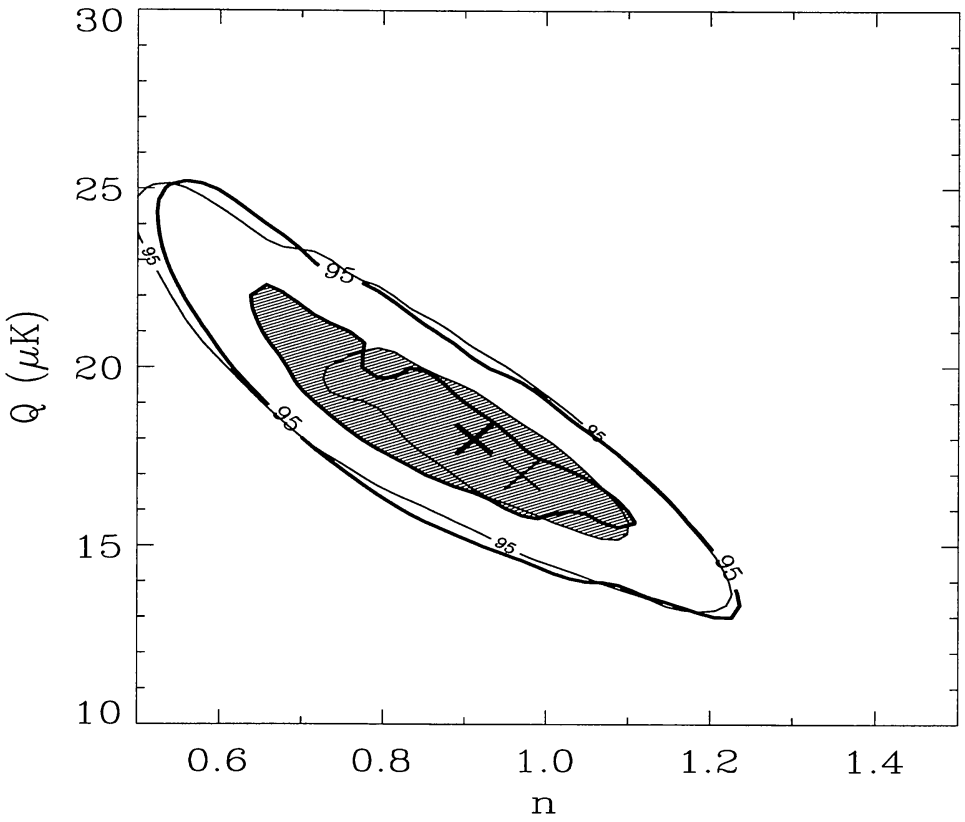

Figure 10. Constraints on n and Q. A precise measurement of the spectral slope n and normalization Q using recent CMB data. $n = 0.93^{+0.17}_{-0.16}$ and $Q = 17.5^{+3.5}_{-2.5}$ μK. See Lineweaver & Barbosa (1997) for further details.

Acknowledgments. I am grateful to my collaborators D. Barbosa, A. Blanchard and J.G. Bartlett. I want to thank Martin Hendry for his Scottish weltanschauang, David Valls-Gabaud for his anxious professionalism, Khalil Chamcham for his international optimism and Hannah Quaintrell for being there. I am also grateful to Nour-Eddine Najid and Idriss Mansouri of the Faculty of Sciences, Ain-Chock, Hassan II University, Casablanca for helpfully arranging my two public lectures. Wayne Hu made several helpful suggestions. I acknowledge support from NSF/NATO post-doctoral fellowship 9552722.